Proc. Natl. Acad. Sci. USA
Vol. 78, No. 4, pp. 1981–1985, April 1981
Applied Physical and Mathematical Sciences

Large-scale flow generation in turbulent convection

(instability/transition/turbulence/large-scale order)

RUBY KRISHNAMURTI* AND LOUIS N. HOWARD†

*Department of Oceanography, Florida State University, Tallahassee, Florida 32306; and †Department of Mathematics, Massachusetts Institute of Technology, Cambridge, Massachusetts 02139

Contributed by Louis N. Howard, January 5, 1981

ABSTRACT **In a horizontal layer of fluid heated from below and cooled from above, cellular convection with horizontal length scale comparable to the layer depth occurs for small enough values of the Rayleigh number. As the Rayleigh number is increased, cellular flow disappears and is replaced by a random array of transient plumes. Upon further increase, these plumes drift in one direction near the bottom and in the opposite direction near the top of the layer with the axes of plumes tilted in such a way that horizontal momentum is transported upward via the Reynolds stress. With the onset of this large-scale flow, the largest scale of motion has increased from that comparable to the layer depth to a scale comparable to the layer width. The conditions for occurrence and determination of the direction of this large-scale circulation are described.**

This is a report on a laboratory study of convection in a horizontal layer of fluid uniformly and steadily heated from below and cooled from above. This is the arrangement that leads to cellular convection for a range of values of the Rayleigh number (the dimensionless measure of temperature difference, defined below) sufficiently small but greater than a critical value. The horizontal scale of these cells is comparable to the depth d of the layer. At successively larger values of this parameter, a number of transitions in the flow pattern as well as in the heat flux are observed (1–6). Most of these changes are within the regime of cellular flows.

We shall describe here a further transition which leads to a very different scale of motion and very different transport properties. In this regime the flow is no longer cellular. It is a flow having primarily two scales of motion. The smaller scale flow, with horizontal scale comparable to the layer depth d, is best described as transient bubbles or plumes that have an organized tilt away from the vertical. The larger scale flow, having scale L, is a horizontal flow with vertical shear such that the flow is oppositely directed near the bottom and the top. L is usually the container width which, in these experiments, is an order of magnitude larger than d. The large-scale flow is apparently maintained against viscous dissipation by the Reynolds stress divergence of the tilted plume motions.

APPARATUS AND PROCEDURE

The convecting fluid occupied a space of depth d and horizontal extent L by L such that d/L was a small number (of order 10^{-2} to 10^{-1}). Most of the new results reported below were obtained with $d = 2$ and 5 cm, $L = 48$ cm. The fluid layer was bounded above and below by metal blocks whose thermal conductivity was several thousand times that of the liquids used. Even in the most extreme case within this set of experiments, when the convective heat flux was 30 times the conductive heat flux, the boundaries had conductivity 2 orders of magnitude higher than the effective conductivity of the fluid layer. Thus, the boundary condition was one of constant temperature along both top and bottom boundaries. On all its lateral boundaries, the fluid layer was bounded and insulated by 3 cm of Plexiglas and 5 cm of Styrofoam. Normally the apparatus was leveled so that its slope was no more than 0.0006 cm in 30 cm. The flatness and parallelism of the horizontal boundaries were comparable to this. The fluids used were water and some of the silicone oils.

The auxiliary equipment for control and measurement of heat flux are described briefly here and in detail in ref. 3. In addition to the convecting layer, six layers of solid materials, each 51 cm square, were used in a stack. The bottom layer was a 10-cm-thick aluminum block with the heater (made of a fine mesh of resistance material) attached to its bottom. Above this lay a 0.64-cm-thick Plexiglas layer and above this a 5-cm-thick copper layer. Above this lay the convecting fluid. Above the fluid were 5 cm of copper, then 0.64 cm of Plexiglas, and then a 10-cm aluminum block containing channels for circulating cooling fluid. (In some of the earlier experiments, 2.5-cm-thick aluminum blocks were used in place of the copper blocks.) The low-conductivity Plexiglas gives rise to measurably large temperature differences between the metal blocks and was used to measure the total heat flux [a method devised by Malkus (1)]. The entire stack was placed in a Plexiglas tank which was surrounded on all sides by Styrofoam 5 cm thick.

The procedure was to set the heater voltage and then adjust the temperature of the cooling water so that, when the temperatures measured in the four metal blocks reached steady state, the mean temperature of the convecting fluid remained at room temperature. Thus, the total heat flux H was prescribed (although not measured) by the input voltage. The temperature was constant on the top and bottom boundaries of the fluid, but the magnitude of the difference ΔT between these constants was determined indirectly through the convective heat flux of the fluid.

The Rayleigh number was computed from the measured ΔT. The total heat flux H through the fluid was equated to the conductive flux through either of the Plexiglas layers. The conductivity of the Plexiglas was determined in terms of the known conductivity of water by performing the experiment with water 0.5 cm deep and ΔT smaller than the critical value for onset of convection.

To study the geometry of the time-dependent flow, the following arrangement was used to obtain (x, t) photographs from which information about the Eulerian velocity could be deduced. Here x refers to the horizontal coordinate along a fixed line within the fluid, perpendicular to the optic axis of the camera, and t refers to the time. We also let y be the coordinate along the optic axis and z the vertical coordinate. The fluid contained suspended tracer particles (small light-reflecting flakes) that became aligned by the shear of the flow. The illuminated region was 2–3 mm in diameter, 48 cm long along x, and chosen to lie near either the bottom or the top of the fluid layer. The

The publication costs of this article were defrayed in part by page charge payment. This article must therefore be hereby marked "*advertisement*" in accordance with 18 U. S. C. §1734 solely to indicate this fact.

lights used were either two 2-W zirconium arc lamps or a 5-mW continuous laser.

With the illuminated region fixed in space, a wedge was moved under the camera in such a way that the camera would rotate about a horizontal axis (parallel to the x axis) through its lens. The resulting photograph showed x along the abscissa and t along the ordinate. For example, if x were a line near the bottom of the layer, perpendicular to the longitudinal axis of roll convection cells, the (x, t) photograph would be as shown in Fig. 2*a*. A tracer particle within the illuminated region and properly oriented so as to send light into the camera produced a mark on the film. Individual particles generally remained in this region long enough to make a short line segment in the picture, as is clearly seen in Fig. 2*a*. The local slope dx/dt of the direction field in the (x, t) photograph produced by these line segments gave the horizontal velocity component as a function of x and t. Cell boundaries, from which fluid is diverging or toward which it is converging, are readily identified not only from this divergence or convergence but from changes in the general brightness or darkness brought about by the tendency of the flakes to become oriented in regions of high shear. In steady convection, as in Fig. 2*a*, cell boundaries remained fixed for all time.

Stray heat sources that might produce lateral temperature gradients were minimized by the physical arrangement of the equipment. The convection tank and the photographic apparatus were enclosed in a light-tight housing. Except for the lights, the motor drive for the camera, and the heater for the fluid layer, all other heat-producing instruments of control or measurement (apart from the experimentalist) were kept outside this housing.

After the large-scale flow was detected, several additions to the apparatus were made to test what controlled the direction of this circulation. The first was a paddle made of 0.32-cm-diameter stainless steel rod, 47 cm long, which could be drawn in the x direction perpendicular to its length. The second addition was a jack to tilt the entire apparatus. The third was the addition of a heater in the side boundary of the fluid layer. A 35-cm length of nichrome wire was embedded in a 0.64-cm-thick sheet of Plexiglas. This sheet replaced a similar one that was part of the side wall. The heater wire occupied a horizontal position approximately 1 cm higher than the bottom of the convecting layer and 1.3 cm outside the fluid.

Finally, the large-scale circulation was also observed in a cylindrical annular tank of fluid uniformly heated below and cooled above. The diameter of the outer Plexiglas cylinder was 45.8 cm, the gap width between the two cylinders was 4.3 cm, and the fluid depth d was 10.6 cm. The lid was floated on an air bearing but restrained from rotating except for tests of the effect of imposed motion of the lid upon direction of large-scale circulation. For cooling the top boundary, the lid carried a volatile fluid open to the air.

OBSERVATIONS

Fig. 1 summarizes some observations of the flow found in the various ranges of the parameters. These parameters are the Rayleigh number R and the Prandtl number P defined as follows:

$$R = \frac{g\alpha}{\kappa\upsilon}\Delta T d^3,\ p = \frac{\nu}{\kappa}$$

where g is the acceleration of gravity, α is the thermal expansion coefficient, κ is the thermal diffusivity, ν is the kinematic viscosity, d is the depth of the fluid layer, and ΔT is the temperature difference between bottom and top boundaries. The new observations refer to flows found to the upper left of the curve labeled V in Fig. 1. To the lower right of this curve the flows are cellular: as labeled, the flow is steady two-dimensional in the range between curves I and II. It is steady three-dimensional cellular between curves II and III, and time-dependent (quasi-periodic), three dimensional, and cellular between curves III and V. By cellular we mean that a fluid parcel initially at some horizontal location is always confined to the vicinity of that location, horizontal excursions being limited by cell boundaries that have horizontal separation comparable to the layer depth. (This is certainly so between curves I and III and at least largely so between curves III and V.) Because most of these states are history dependent, the actual transition point varies depending upon how it was attained. Fig. 1 obtains when the state of the system was reached from lower values of Rayleigh number, by small increments in R. Further explanation can be found in ref. 5.

Curve V was defined in ref. 2 as the Rayleigh number above which irregular fluctuations in temperature at a point mid-depth in the fluid layer were nearly always present. Although somewhat subjective, it is a useful criterion.

One of the major differences between the flows occurring to the upper left of curve V and those to the lower right is seen in the (x, t) photographs in Fig. 2. Fig. 2 *b* and *c* show a line in the fluid layer 0.2 cm above the bottom boundary. Fig. 2*b*, at $R = 10^6$ and $P = 0.86 \times 10^3$, is for parameter values to the right of curve V. Fig. 2*c*, at $R = 10^6$ but $P = 7$, is to the left of curve V. In Fig. 2*b* there are cell boundaries which, although they may oscillate laterally, are always identifiable. In Fig. 2*c*, there are no cell boundaries. Fig. 2*b* is a cellular flow with bright or dark regions moving repeatedly from one cell boundary to a neighboring one. These regions have been shown (5) to correspond to hot or cold spots convected around the cell. In Fig. 2*c*, hot bubbles or plumes off the bottom, randomly spaced in position and time, form and vanish. Cold bubbles off the top likewise form and vanish, much as described by the bubble model (7). At any instant of time, their horizontal spacing is approximately d or somewhat less. It should be pointed out also that Fig. 2*c* is not an initial transient state; it is the statistically steady state that is observed 1 hr or 100 hr after convection is started.

At $P = 7$ and $R = 5 \times 10^4$, the flow is similar to Fig. 2*b*, so that increasing R at fixed P also leads to the change of flow depicted from Fig. 2*b* to Fig. 2*c*.

The other major difference—and the one to which we particularly wish to call attention in this report—is seen in Fig. 2*d* which shows an (x, t) photograph for $P = 7$ and $R = 2.4 \times 10^6$, taken 0.2 cm above the bottom boundary. It shows that the plumes have a net drift from left to right with an average speed of 7×10^{-2} cm sec^{-1}. A similar photograph taken 0.2 cm below the top showed plumes drifting from right to left with the same average speed.

From the (x, t) photographs it is not known if this apparent motion is a wave propagation or if there is an associated mass flux. Thymol blue was added to the water so that neutrally buoyant dye could be produced at an electrode, and the dyed fluid was followed with time. Fig. 3 shows a sequence, at 30-sec intervals, of a vertical slice (x, z) view of the fluid. In this case the layer depth was 10 cm. The dye front along the bottom progressed at an average speed $\bar{u}$ of 3×10^{-2} cm sec^{-1} from left to right and actually reached the opposite wall, by which time it was quite diffuse. These magnitudes are not easily compared from case to case because only the x component, $\bar{u}$, is measured, whereas in some repetitions of the experiment there was a velocity component $\bar{v}$ in the y direction as well. Maximum values of $\bar{u}$ on the order of 10^{-1} cm sec^{-1} have been observed.

In Fig. 3, as the dyed fluid became buoyant, it rose into the interior of the layer where it became entangled in the motion of the plume. It often rose to become caught in the leftward drift

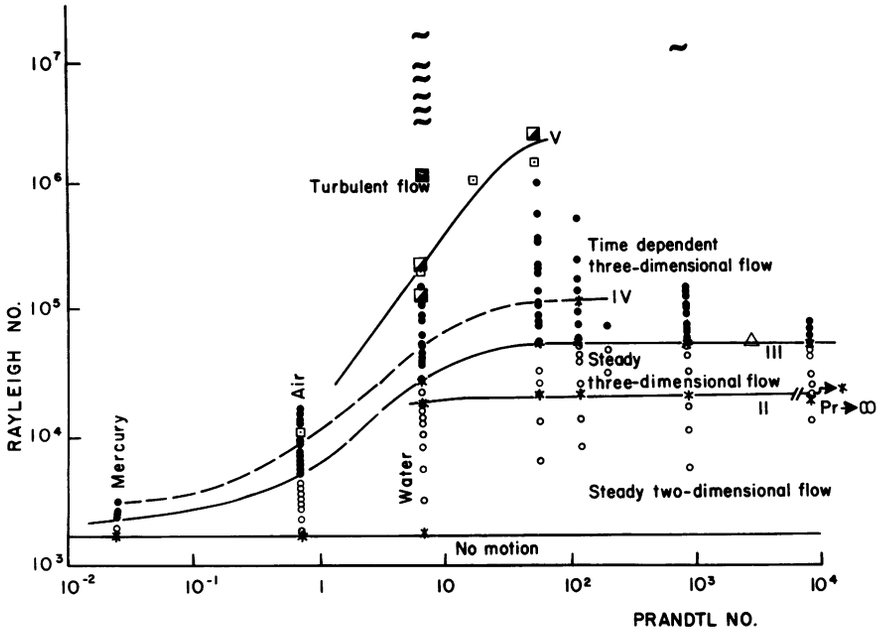

FIG. 1. Regime diagram. ○, Steady cellular flow; ●, time-dependent cellular flow; ◪, cells and transient bubbles (transitional); ■, transient bubbles; ∼, large-scale flow with tilted plumes; *, heat flux transitions (see text and ref. 5 for further explanation).

at the top of the layer. A general tilt of the plumes from lower right to upper left can be discerned even though the flow was quite turbulent. Thus, we conclude that there is not only a (time and/or horizontal) mean Eulerian velocity $\bar{u}(z)$ but also a net horizontal Lagrangian transport extending the entire width of the tank. Observations of the occurrence of cells, plumes, and large-scale flow in various regions of parameter space are summarized in Fig. 1.

On repetitions of the experiment, the large-scale flow was seen to be sometimes from left to right along x at the bottom and from right to left along x at the top ($\bar{u}$ counterclockwise). On other realizations, the flow was clockwise. On still others, the large-scale flow was in the y direction ($\bar{v}$) and either clockwise or counterclockwise. It may also be at some other angle to the x direction. When the flow was $\bar{u}$ and clockwise, this flow was often nearly independent of y but, on another repetition, it might be that the center of the large-scale rising was at the left wall at some value of y; at other values of y, the center of the rising wandered to other values of x.

When this large-scale flow was first discovered, various tests were made to see if it were inadvertently being driven directly by horizontal asymmetries. The leveling of the apparatus was checked. Horizontal temperature gradients in the boundaries were measured to check the possibility of malfunction of the cooling or heating system. In the aluminum blocks with the heater, or the cooler, horizontal gradients were of order 10^{-3}°C across 35 cm. In the middle two (copper) blocks, which do not contain any thermal forcing, the horizontal gradients were larger: 10^{-2}°C in 25 cm. However, this magnitude of horizontal gradient would drive, in water, a horizontal velocity $u \approx 10^{-3}$ cm sec^{-1} which is 2 orders of magnitude smaller than observed. Although horizontal asymmetries certainly must be present, due to errors in leveling the apparatus or to small differences in temperature of the Plexiglas side walls, these had no observable effect at lower Rayleigh number, or even at the same Rayleigh number (with the same ratio of side wall area to horizontal area), when a higher Prandtl number fluid was used and no large-scale flow was observed.

Convinced that the large-scale flow was not externally driven, we attempted to check, as to order of magnitude, that the large-scale flow and the tilt of the plumes were consistent with the Reynolds equations relating a (time- and horizontal-) mean flow with the Reynolds stress associated with fluctuations. The principal equation here is the mean horizontal momentum equation which, if the tank were horizontally unbounded (or in the case of the cylindrical annulus), is:

$$(\overline{u'w'})_z = \nu \bar{u}_{zz}. \qquad [1]$$

The overbar indicates a horizontal and time average, u' and w' are the fluctuations from the mean, and ν is the kinematic viscosity. (With the finite horizontal extent there could conceivably also be a nonzero mean horizontal pressure gradient term in this equation—which indeed might well be important were there external driving—but we omit this here.) Integrating vertically from the bottom wall we obtain $\overline{u'w'} = \nu(\bar{u}_z - \bar{u}_z^w)$, $\bar{u}_z^w$ being the mean shear at the wall. Now, for a rough estimate we may perhaps suppose that the mean flow $\bar{u}$ has a profile in z something like $\bar{u} = -U \sin(2\pi z/d)$, taking the origin of z at the center of the fluid layer so $-d/2 < z < d/2$. This would correspond to a Reynolds stress $\overline{u'w'} = (4\pi U\nu/d)\cos^2(\pi z/d)$. Thus, with $U \geq 0$, corresponding to flow from left to right in the lower half of the layer (as in Fig. 3), $\overline{u'w'}$ must be negative and its maximal magnitude, achieved at the center, should be about $10\nu/d$ times the maximum of $\bar{u}$. Detailed measurements of the fluctuating velocity components u' and w', and of their correlation, have not yet been made. However visual observation and photographs like Fig. 3, together with the (x, t) photographs, indicate the following. (*i*) The fluctuations are on the whole associated with motions in the tilting plumes. (*ii*) The plumes tilt in such a way (about 45° from lower right to upper left in cases such as shown in Fig. 3) that $\overline{u'w'}$ has sign opposite to that of $\bar{u}$ in the lower half and w' is characteristically of about the same magnitude as u'. (*iii*) The maximal magnitudes of u', w', and $\bar{u}$ all are about 0.1 cm sec^{-1} in our experiments in which the large-scale flow is observed.

We thus may estimate $\overline{u'w'}$ as about 0.2×10^{-2} cm^2 sec^{-2} if we include factors of about 1/2 for the x average (assuming u' and w' have sinusoidal variation with x) and also for the time average. The last is a rough estimate from the fraction of the time that plumes are seen at any location on the (x, t) photographs. With $d = 5$ cm and $\nu = 0.01$ cm^2 sec^{-1} we get $(10\nu/d)u_{max} \approx 0.2 \times 10^{-2}$ cm^2 sec^{-2}, so there does not appear to be any clear inconsistency with the Reynolds equation (Eq. 1). One may regard the mean flow as being "driven" by the Reynolds stress associated with the tilting plumes. We emphasize that such a

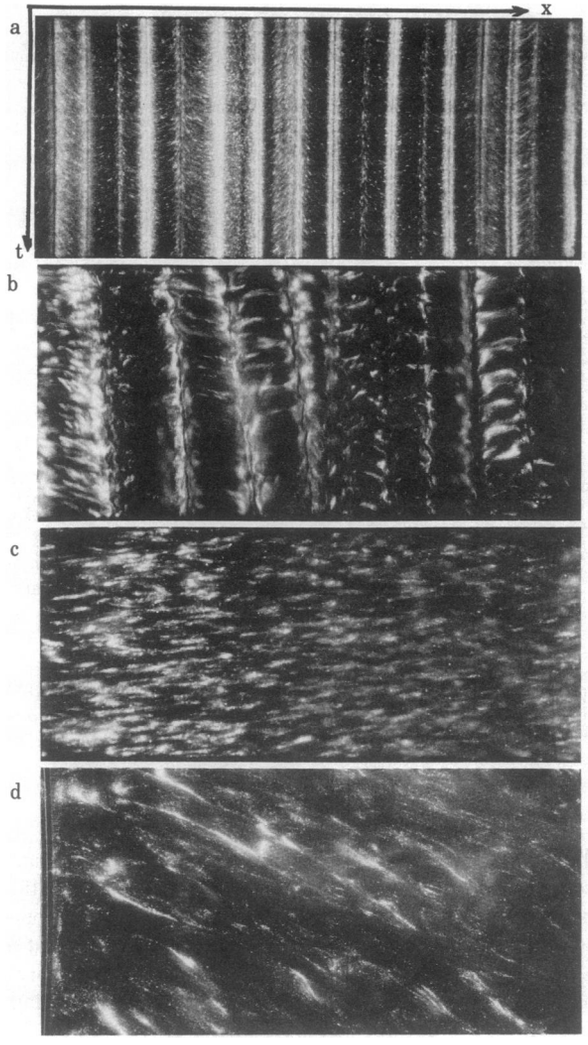

FIG. 2. (x, t) representations of the flow 0.2 cm above the bottom boundary. The range in x along the abscissa is 0 to 45 cm; t increases downward; range in time is 0 to τ. (*a*) $R = 7.5 \times 10^4$, $P = 0.86 \times 10^3$, $\tau = 17$ min. (*b*) $R = 10^6$, $P = 0.86 \times 10^3$, $\tau = 22$ min. (*c*) $R = 10^6$, $P = 7$, $\tau = 22$ min. (*d*) $R = 2.4 \times 10^6$, $P = 7$, $\tau = 9$ min.

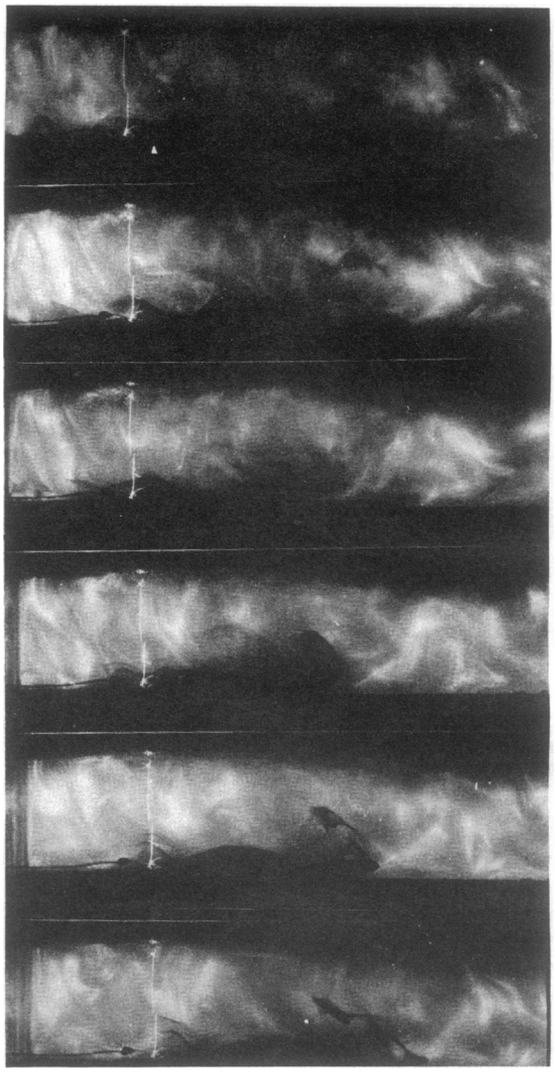

FIG. 3. Sequence of views of (x, z) slice through convecting fluid, showing the rightward progress of dye along bottom and the lower right to upper left tilt of plumes.

statement is a description, not an explanation, of the large-scale flow. The Reynolds equation would also be consistent with no mean flow, and no tilting of the plumes—and in fact this appears to be what occurs below a Rayleigh number of about 2×10^6 in water. The theoretical understanding of why this transition occurs and why it occurs at $R = 2 \times 10^6$ remains a challenge.

The phenomenon seems to resemble the onset of steady convection in that the physically realized "state" changes to one of a set, each member of which individually has less symmetry than the equations and boundary conditions describing the motion. Such symmetry-breaking occurs in many mathematical models involving changes of stability of stationary or periodic solutions and associated bifurcations, and Rayleigh's explanation of the onset of cellular convection in such terms has been followed in spirit by essentially all of the many subsequent explorations of other aspects of cellular convection. Whether such concepts as stability and bifurcation can contribute usefully to an understanding of a transition entirely in the turbulent range seems less clear; this report, in any case, is about the observation of the transition, not its theoretical interpretation.

What determines the direction of the large-scale flow? We were not successful in altering the direction of the established large-scale flow by drawing the paddle along the bottom of the convecting layer, although we tried various speeds including one approximately the speed of the large-scale flow. We did not attempt this while the Rayleigh number was being increased through $R \approx 2 \times 10^6$. It was not possible to match the time scales involved. Similarly, in the annular tank it was not possible to alter the direction of the already established large-scale flow by rotating the lid through one revolution, at various speeds, in either the clockwise or counterclockwise direction.

When the entire convection tank was tilted at various angles up to a maximum of 0.23 degrees, neither the already established large-scale flow nor the large-scale flow that set in as R was increased from zero to $>2 \times 10^6$ was determined by the tilt of the layer. Certainly it is known that, if the tilt angle is large enough, the direction of the flow is determined by that tilt but for the tilts used here (which were 10^2 times larger than any tilt of the layer due to leveling error) there was no such determination.

When the fluid layer was heated from the side, the direction of the large-scale flow could be determined when the heating rate was large enough. Several different heating rates were tried. For example, when the power to the side heater was 3 W, this heating rate did not reverse an already established large-

scale flow. The rising motion induced at the heated side wall was accompanied by sinking motion a short distance ($<d$) away, and the rest of the layer behaved as without the side heating. When the side heater, at 3 W, was on while R was increased from zero through 2×10^6, the direction of the large-scale flow was not determined by the side on which the heater was placed. However, when the heating was at 11 W, as R was increased from zero to 2×10^6 the large-scale flow was $\tilde{u}$, clockwise, when the heater was on the left, and $\tilde{u}$, counterclockwise, when the heater was on the right.

Furthermore, at 11 W, an established large-scale flow could be made to reverse direction by switching the heater to the other side of the tank. The response was within an hour; the thermal diffusion time of the Plexiglas spacer was approximately one-half hour. Also, after the side heater was turned off, the direction of the large-scale flow remained unchanged for several days thereafter. This was with $R = 10^7$. The heating at 11 W caused an increase in temperature of approximately 1°C at the outside of the Plexiglas spacer, about 1 cm from the fluid. The temperature difference in the vertical was 2°C. This heating alone, with the vertical Rayleigh number $R = 0$, produced a large-scale overturning with horizontal velocity $u(x)$ measured at a distance $z = 0.2$ cm below the top of the 5-cm-deep layer. The measurement was conveniently made from the slopes of particles in an (x, t) photograph. The maximum u, which occurred at $x = 14$ cm from the heated wall, for $z = 0.2$ cm, was 8×10^{-3} cm sec^{-1}. This is still 1 order of magnitude less than the $\tilde{u}$ produced by the tilting plumes.

Finally, large-scale flow was observed in the cylindrical annulus, showing that a pressure difference between two lateral boundaries is not necessary to produce this flow. The small-scale plumes were considerably narrower than the depth d of the layer, but they tilted approximately 45° and in this sense they occupied a horizontal distance of about d. The large-scale flow was observed to continue around the annulus, in one direction near the bottom and in the opposite direction near the top. With the geometry thus unbounded in x, the large-scale flow has horizontal wave number 0.

Movies of the flow in the annulus and of an (x, z) slice in the square tank are available.

The heat flux, nondimensionalized to equal the Nusselt number times the Rayleigh number, is plotted against Rayleigh number in Fig. 4. (The Nusselt number is the ratio of total heat flux to conductive heat flux.) Discrete changes in slope were seen at Rayleigh numbers $R_{III} = 3.3 \times 10^4$, $R_{IV} = 5.5 \times 10^4$, $R_V = 1.0 \times 10^5$, $R_{VI} = 5.0 \times 10^5$, and $R_{VII} = 1.1 \times 10^6$, the last three of which are shown in Fig. 4. Some of these are in good agreement with the Malkus heat flux transitions $R_{III} = 3 \times 10^4$, $R_{IV} = 5.5 \times 10^4$, $R_V = 1.7 \times 10^5$, $R_{VI} = 4.1 \times 10^5$, $R_{VII} = 8.5 \times 10^5$, and $R_{VIII} = 1.6 \times 10^6$. It appears that the onset of the large-scale circulation might be associated with the slope change at $R_{VII} = 1.1 \times 10^6$.

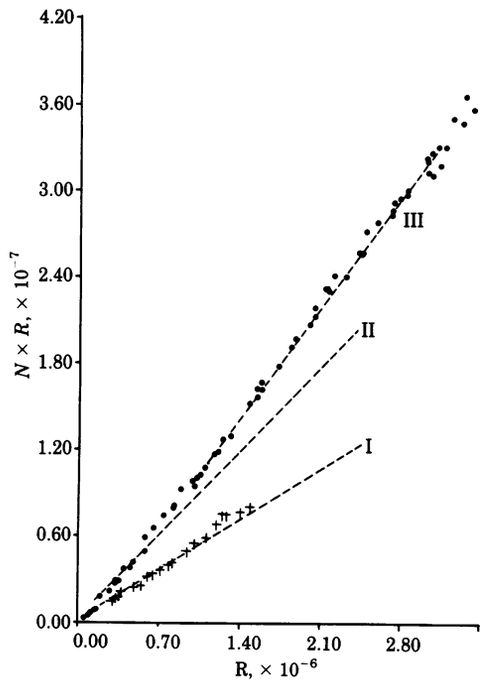

FIG. 4. Heat flux H vs. Rayleigh number R. H has been nondimensionalized to equal $N \times R$ (N is the Nusselt number). The coordinate scale is appropriate for the data shown by dots. For +, the scale should be decreased by a factor 10. A least-squares fit of segments of data to a straight line $NR = aR + b$ gave $a = 5.05$ for the line labeled I, $a = 8.40$ for II, and $a = 10.7$ for III. The change in slope at R = 1.1 $\times 10^6$ may be associated with the onset of the large-scale circulation which is seen at $R \geq 2 \times 10^6$.

DISCUSSION

As the Rayleigh number is increased, cellular flow vanishes and is replaced by a flow that has no permanent cell boundaries. It consists of hot rising and cold sinking transient bubbles or plumes. At still higher R, the plumes drift in one direction near the bottom, in the opposite direction near the top of the layer, and tilt from the vertical and thereby transport mean horizontal momentum in the vertical direction. When viewed in the (x, t) representation, the transition is reminiscent of a phase transition. When there are cell boundaries as in Fig. 2*a*, fluid parcels are forever confined to circulate in the lattice-like confines of the cell walls. In Fig. 2*b*, plumes appear but are constrained by the cell walls to circulate within the cell. In Fig. 2*c* the cell boundaries have vanished and, as R is increased further in Fig. 2*d*, the "melt" begins to flow. The largest scale of motion which was previously equal to the depth d has suddenly changed to the layer width L. The appearance of this new large scale has many implications. Turbulent horizontal transport of a passive tracer is completely changed when this large-scale flow sets in. Continental drift and sea floor spreading, which have generally been thought to require deep convection in the mantle to explain the large scales observed at the crust, might perhaps be viewed in terms of a large-scale convective flow in the much shallower but more plastic asthenosphere.

This work was supported by the Fluid Dynamics Division of the Office of Naval Research and by the National Science Foundation (Grant OCE-772-7939). This is Geophysical Fluid Dynamics Institute contribution 162.

1. Malkus, W. V. R. (1954) *Proc. R. Soc. London Ser. A* **225**, 185–195.
2. Willis, G. E. & Deardorff, J. W. (1967) *Phys. Fluids* **10**, 931–937.
3. Willis, G. E. & Deardorff, J. W. (1967) *Phys. Fluids* **10**, 1861–1866.
4. Krishnamurti, R. (1970) *J. Fluid Mech.* **42**, 295–307.
5. Krishnamurti, R. (1970) *J. Fluid Mech.* **42**, 309–320.
6. Busse, F. H. & Whitehead, J. A. (1971) *J. Fluid Mech.* **47**, 305–320.
7. Howard, L. N. (1966) *Proceedings of the Eleventh International Congress of Applied Mechanics*, Munich, Federal Republic of Germany, August 1964, ed. Görtler, H. (Springer, Berlin), pp. 1109–1115.